OPEN ACCESS
IOP Publishing
Journal of Physics D: Applied Physics
J. Phys. D: Appl. Phys. **51** (2018) 125306 (8pp)
https://doi.org/10.1088/1361-6463/aaac64

In situ monitoring of atomic layer epitaxy via optical ellipsometry

F Lyzwa[1,2], P Marsik[2], V Roddatis[3], C Bernhard[2], M Jungbauer[1] and V Moshnyaga[1]

[1] I. Physikalisches Institut, Georg-August-Universität Göttingen, Friedrich-Hund-Platz 1, 37077 Göttingen, Germany
[2] Department of Physics and Fribourg Center for Nanomaterials, University of Fribourg, Chemin du Musée 3, CH-1700 Fribourg, Switzerland
[3] Institut für Materialphysik, Georg-August-Universität Göttingen, Friedrich-Hund-Platz 1, 37077 Göttingen, Germany

E-mail: fryderyk.lyzwa@unifr.ch

Received 30 October 2017, revised 9 January 2018
Accepted for publication 1 February 2018
Published 6 March 2018

Abstract

We report on the use of time-resolved optical ellipsometry to monitor the deposition of single atomic layers with subatomic sensitivity. Ruddlesden–Popper thin films of $SrO(SrTiO_3)_{n=4}$ were grown by means of metalorganic aerosol deposition in the atomic layer epitaxy mode on $SrTiO_3(1\,0\,0)$, LSAT(1 0 0) and $DyScO_3(1\,1\,0)$ substrates. The measured time dependences of ellipsometric angles, $\Delta(t)$ and $\Psi(t)$, were described by using a simple optical model, considering the sequence of atomic layers SrO and TiO_2 with corresponding bulk refractive indices. As a result, valuable online information on the atomic layer epitaxy process was obtained. *Ex situ* characterization techniques, i.e. transmission electron microscopy, x-ray diffraction and x-ray reflectometry verify the crystal structure and confirm the predictions of optical ellipsometry.

Keywords: atomic layer epitaxy, *in situ* growth monitoring, optical ellipsometry, Ruddlesden–Popper, transmission electron microscopy

S Supplementary material for this article is available online

(Some figures may appear in colour only in the online journal)

1. Introduction

Nanoscience and modern material physics are based on the growth and study of thin films with thicknesses spreading down to one atomic layer (monolayer, ML). Several phenomena of great current interest are coupled to this scale, e.g. high mobility electron gas at the interface between the insulator $LaAlO_3$ and $SrTiO_3$ (STO) [1], high temperature superconductivity in a FeSe monolayer on an STO substrate [2, 3], interfacial ferromagnetism [4] and strain-engineering to obtain ferroelectric properties in STO [5]. To fabricate those systems several deposition techniques can be employed, including molecular-beam epitaxy (MBE), pulsed laser deposition (PLD) and chemical vapor deposition (CVD). Therefore, the growth monitoring process itself is of great importance in order to control the successful film growth and, finally, to gain information on the electronic properties, defect formation, interfacial reconstructions etc. already during the growth itself.

Different methods have been used to monitor the growth of thin films. The most common approach is 'reflection high-energy electron diffraction' (RHEED), in which the interference pattern of reflected electrons upon the film surface is detected. Complete unit cells (u.c.) or sometimes half u.c. can be observed, depending on the material system. However, one can only distinguish between the different growth modes such as island or layer-by-layer growth, but hardly identify what kind of material is deposited. This method is also limited to ultrahigh vacuum (UHV) deposition conditions. In addition,

an *in situ* x-ray technique such as 'grazing-incidence small-angle x-ray scattering' (GISAXS) [6] enables to derive the film growth mode, the average particle shape and size as well as to probe film surfaces and interfaces with high sensitivity and dynamics. However, to avoid light scattering an UHV setup is required, which has to be coupled to a synchrotron source to provide a well-collimated, monochromatic incident beam with very high intensity. Optical probe techniques such as reflectance-difference spectroscopy (RDS), p-polarized reflectance spectroscopy and spectral ellipsometry (SE) [7, 8] are advantageous because of their noninvasive and non-destructive character, as well as due to their compatibility to non-vacuum chemical deposition methods. With these spectroscopic techniques, information about the film thickness, optical properties and surface morphology can be extracted.

Nevertheless, the reflected signal is usually not detected in a continuous mode during the film growth, but rather after each growth step. Real-time monitoring for the growth of semiconductor films was previously reported e.g. by Zettler *et al* [9], by means of SE in the rotating analyzer ellipsometer (RAE) configuration with a monochromator placed in the beam path, suffering from a relatively low signal-noise ratio (SNR). Using a laser as the probe light improves the SNR, as was shown e.g. by Lee & Masumoto [10] or Zhu *et al* [11]. In the latter study, *in situ* ellipsometry was compared to RHEED, where a good agreement between these two monitoring techniques for an interrupted growth cycle and full u.c. of an STO thin film on an STO substrate was established. In later publications, they developed a relatively complex mean-field theory to describe the optical response [12, 13]. In our previous study [14], we have shown that by using an ellipsometry setup in the polarizer-photoelastic modulator-sample-analyzer (PMSA) configuration one can detect the evolution of the optical ellipsometry signal during the deposition of atomic layers in real-time. The following questions arise: (1) can we monitor/control the growth of oxides in general down to the submonolayer level in real-time, (2) what kind of optical model is able to describe the growth process and (3) which information can be obtained from modeling the experimental data?

Here, by using the above mentioned experimental setup, we performed a detailed study of the heteroepitaxial growth of the Ruddlesden–Popper (RP) series Sr–O[Sr–O/Ti–O_2]$_{n=4}$ (RP-STO) in the atomic layer epitaxy (ALE) mode. Moreover, the change of the ellipsometric signal during the ALE growth monitoring was described by a relatively simple model considering optical constants of neutral sub-monolayers of Sr–O and Ti–O_2, as building blocks of the RP system (see figure 2(c)). The information obtained from *in situ* ellipsometry was verified by *ex situ* characterization of the crystal structure by means of transmission electron microscopy (TEM), x-ray diffraction (XRD) and reflection (XRR).

2. Sample preparation and ellipsometry model

All samples were prepared by means of a metalorganic aerosol deposition (MAD) technique [15]. In order to grow atomic layers of Sr–O and Ti–O_2 on top of each other, the precursors Sr(acetylacetonate)$_2$ (P_{Sr}) and Ti(isoprop)$_2$(tetramethylheptanedionate)$_2$ (P_{Ti}) were first dissolved separately in dimethylformamide (DMFA). Each precursor solution was sequentially sprayed by means of a pneumatic nozzle (droplet size ~20 μm) using compressed air onto a heated substrate, T_{sub} ~ 900 °C, where a heterogeneous pyrolysis reaction occurs. The volumes of each precursor solution and, hence, the thickness of the layers were controlled in separate pulses via a precision pump system, resulting in deposition rates of $r = 0.06$–9.5 ML s^{-1}. In between the Sr–O and Ti–O_2 pulses (atomic layers) we chose a delay time of 6–8 s. Prior to deposition, the STO substrates were TiO_2-terminated in order to remove the top Sr–O layer at the substrate surface, as described in [16]. Typical atomic force microscopy (AFM) images of an STO substrate and an RP-STO film (see supplementary material (stacks.iop.org/JPhysD/51/125306/mmedia)) reveal the root mean square roughness, RMS = 0.1 nm and 1.44 nm, respectively. The LSAT ($(La_{0.3}Sr_{0.7})(Al_{0.65}Ta_{0.35})O_3$) and $DyScO_3$ substrates were not surface treated prior to deposition. Due to a relatively high substrate temperature, T_{sub} ~ 900 °C, and highly oxidizing conditions, we can be sure to have no contamination at the substrate surface and that all substrates are equally clean.

The *in situ* growth control was performed by means of an optical ellipsometry setup in the PMSA-configuration as described in detail in [14]. A HeNe-Laser beam ($\lambda = 632.8$ nm) was aligned close to the Brewster angle, $\phi_B = 62°$, with respect to the substrate normal. Polarizer and analyzer angles were both set to 45°. The polarization of the light was modulated at a frequency of $\omega = 50$ kHz by means of a photoelastic modulator placed between the polarizer and the sample. The resulting modulation of the light intensity, detected with a photodiode via a lock-in technique, was used to derive the ellipsometric angles Ψ and Δ, given by the ratio ρ of the Fresnel coefficients $r_{(s,p)}$:

$$\frac{r_p}{r_s} = \rho = \tan\Psi \cdot e^{i\Delta}$$
$$\Rightarrow \quad \Delta = \tan^{-1}\left(\frac{\mathrm{Im}\,\rho}{\mathrm{Re}\rho}\right) \quad \text{and} \quad \Psi = \tan^{-1}\left(|\rho|\right). \quad (1)$$

The time-resolved optical response (Δ, Ψ) of a thin film during the growth as a function of time or film thickness was theoretically described by using a standard transfer matrix formalism (for *s*- and *p*- components), which couples the incident (i), reflected (r) and transmitted (t) amplitudes of the electric field vector E for an isotropic, homogeneous sample [17]:

$$\begin{bmatrix} E_i \\ E_r \end{bmatrix} = \widehat{M} \cdot \begin{bmatrix} E_t \\ 0 \end{bmatrix}. \quad (2)$$

Imagine now, we deposit a layer A with a complex refractive index, $\tilde{n}_A$, and thickness, d_A, on top of a substrate (see figure 1). We can express E at the interface ambient air and layer A (amb/A) by a 2×2 matrix $R_{amb/A}(r_{(s,p)}, t_{(s,p)})$, composed by the Fresnel coefficients. The wave traveling through the layer A is expressed also by a 2×2 matrix, $\phi_A(\tilde{n}_A, \theta_2, \omega, d_A)$. Here, θ_2 is the angle under which the wave is traveling through the layer and ω is the photon energy.

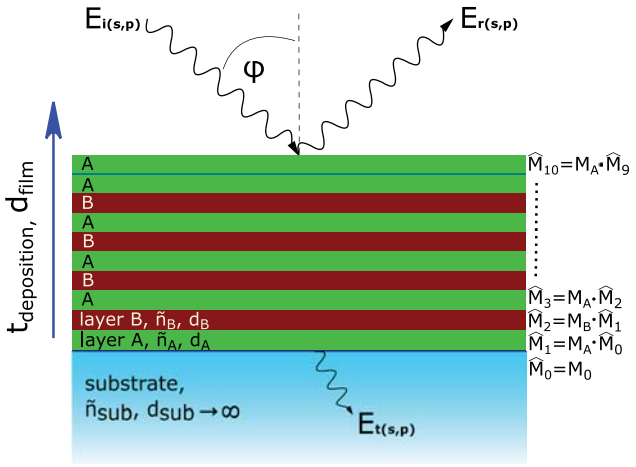

Figure 1. Schematic of the sample and the ellipsometry modeling. The film shown consists of 4 u.c. of STO (A = SrO, B = TiO_2) with an SrO-extra layer on top.

The total optical response of the material is described by the matrix $\widehat{M}_1$, which is determined by the contribution of the substrate and the layer A. Using $R_{\mathrm{A/amb}} \cdot R_{\mathrm{amb/B}} = R_{\mathrm{A/B}}$, we can describe a free standing layer A and derive:

$$\begin{bmatrix} E_i \\ E_r \end{bmatrix} = \underbrace{R_{\mathrm{amb/A}} \cdot \phi_{\mathrm{A}} \cdot R_{\mathrm{A/sub}}}_{\widehat{M}_1} \cdot \begin{bmatrix} E_t \\ 0 \end{bmatrix}$$

$$= \underbrace{R_{\mathrm{amb/A}} \cdot \phi_{\mathrm{A}} \cdot R_{\mathrm{A/amb}}}_{M_{\mathrm{A}}} \cdot \underbrace{R_{\mathrm{amb/sub}}}_{M_0} \cdot \begin{bmatrix} E_t \\ 0 \end{bmatrix}. \qquad (3)$$

We assume $d_{\mathrm{sub}} \to \infty$, since we expect a negligible contribution from the backscattered light also due to the fact that the substrates are only one-side polished.

An additional layer B with properties ($\tilde{n}_{\mathrm{B}}$, d_{B}) creates a different set of matrices ($R_{\mathrm{amb/B}}, \phi_{\mathrm{A}}, R_{\mathrm{B/amb}}$), and the obtained response is given by $\widehat{M}_2 = M_{\mathrm{B}} \cdot \widehat{M}_1$.

According to the RP series, we alternate M_{A} and M_{B} and calculate the optical response as

$$\widehat{M}_j = M_j \cdot \widehat{M}_{j-1} \qquad (4)$$

for j numbers of deposited layers. Using equation (1) we obtain the theoretical values (Δ, Ψ) for any film thickness/deposition time, since the Fresnel coefficients $r_{(s,p)} = \frac{E_{r(s,p)}}{E_{i(s,p)}} = \frac{m_{21(s,p)}}{m_{11(s,p)}}$ are described by the elements of the matrix $\widehat{M}_j$.

In order to confirm the presence of the RP structure in the grown films, an additional *ex situ* structural characterization was done by means of XRD in the $\theta - 2\theta$ geometry and XRR, using a D8 Advance diffractometer from Bruker AXS. The analysis of the atomic structure of the films was performed by high-resolution scanning transmission electron microscopy (HR-STEM) and electron energy loss spectroscopy (EELS). The TEM samples were prepared by mechanical polishing followed by Ar^+ ion milling at 4 kV down to 0.5 kV until electron transparency was achieved. HR-STEM images were recorded with parallel beam illumination using a FEI Titan 800–300 environmental TEM operated at 300 kV acceleration voltage. The microscope is equipped with a Gatan Image Filter Quantum 965ER. Spectrum images (SI) were collected to confirm chemical composition of the RP planar defects.

3. Results and discussion

In figure 2(a) the time evolution of the measured ellipsometric angle, Δ, for an RP-STO film on an STO-substrate is presented. The inset shows an enlarged view of the time evolution during the deposition of a single Ti–O_2/Sr–O cycle. Note that after the deposition of one Ti–O_2 atomic layer, a 6 s pause in the growth process (marked in orange color) was applied, before a Sr–O atomic layer is deposited. During this time, even though no further material is deposited, a change in Δ can still be seen, possibly due to macroscopic structural reorganization via surface reactions (e.g. oxidation).

The corresponding simulation as a function of the film thickness is shown in the bottom panel of figure 2(a). As starting parameters for the modeling we used room temperature values of the refractive index, $\tilde{n}$, of the bulk SrO and TiO_2 (rutile) materials [18]. These values were then slightly adjusted to better reproduce the experimental data, with final deviations of −0.1% for SrO and 1.2% for TiO_2. These small differences are likely due to the elevated substrate temperatures during deposition (~900 °C) and possibly due to different film and bulk optical constants. The value of $\tilde{n}$ for the substrate has been derived from the measured Δ, Ψ-values before the deposition started. All values, as well as the atomic layer thicknesses, are listed in table 1. Note that the reduction of Δ at a higher film thickness arises from the interference of the laser beam, reflected at the film/amb and substrate/film interfaces. This interference effect is reproduced by our simulations for the ideally grown film.

Two major deviations of the ideal model growth from the experimental data can be seen: (1) during the growth of a 4 u.c. stack of STO the phase shift angle Δ changes by about $\Delta^{4\mathrm{STO}} = 0.36°(2)$, which is rather reproducible throughout the whole measurement. The only exception occurs for the very first stack at the start of the deposition (red square), for which the amplitude of $\Delta^{4\mathrm{STO}} = 0.18(2)$ is reduced by a factor of two, suggesting that only half of Sr–O and Ti–O_2 atomic layers are deposited here. Correspondingly, in the simulation for the first stack only half of the atomic layer thicknesses were considered, i.e. $d_{\mathrm{SrO}} \to \frac{d_{\mathrm{SrO}}}{2}, d_{\mathrm{TiO_2}} \to \frac{d_{\mathrm{TiO_2}}}{2}$. We assume that this slower growth at the very beginning of the deposition might be related to a lower surface mobility and reduced adsorption of the reactants on the bare STO substrate. This leads to an incomplete first layer with Sr–O islands separated by gaps, closing during the next Ti–O_2 pulse. An additional Sr–O layer compensates this process and increases the adsorption. (2) For the first 10–12 nm of the film—this region will be called transition zone (TZ) from now on—the experimental data deviate slightly from the modeled curve in the overall shape as well as in a small horizontal drift during a 4 u.c.-STO repetition. A reason for this difference in $\tilde{n}$ can be small deviations from the ideal monolayer doses, since the stoichiometry must not necessarily stay constant during the entire growth process. A possible explanation is that SrO diffuses into the

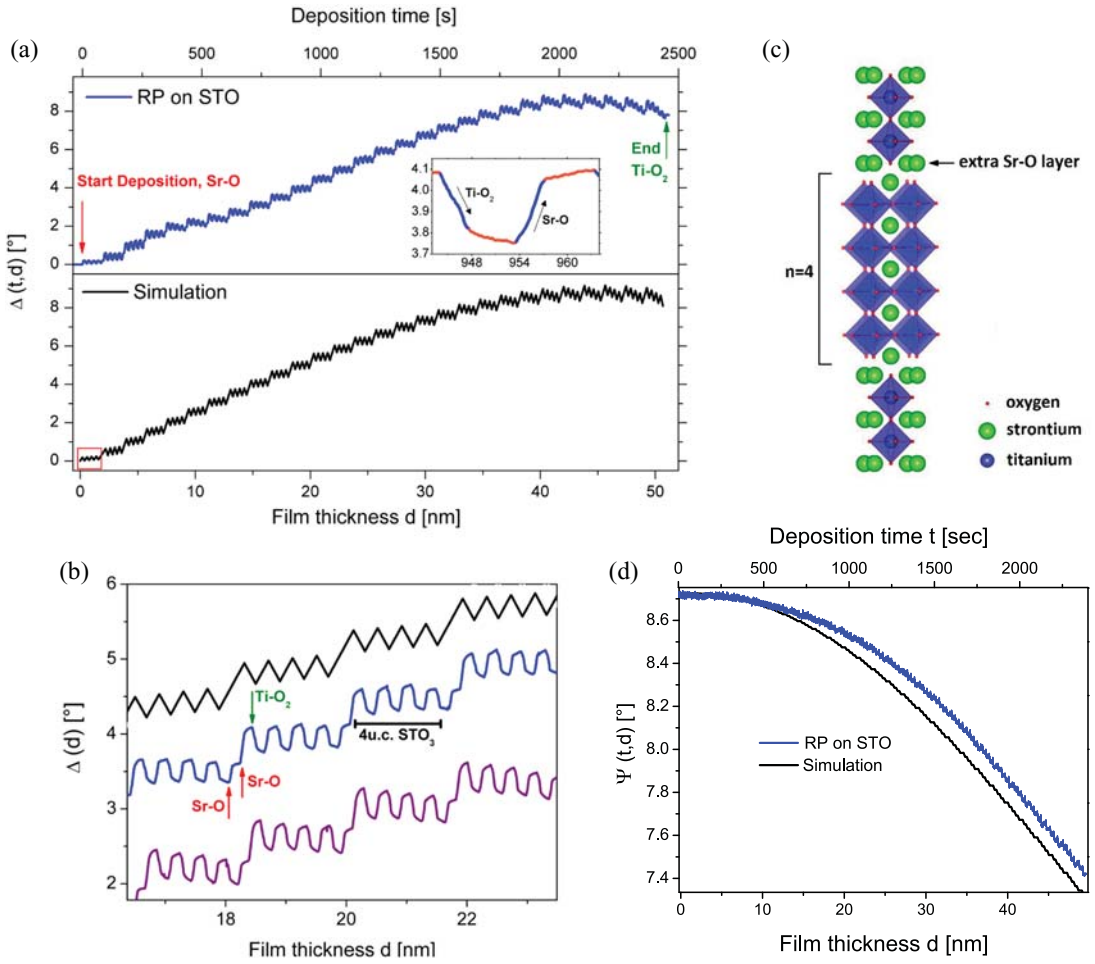

Figure 2. (a) Top-panel: time evolution of the ellipsometric angle, Δ, as measured during the growth of an RP film on STO (0 0 1) with $N = 28$ repetitions (blue curve). The inset details the evolution during the deposition of one Sr–O and one Ti–O_2 atomic layer. The pause in between each of the pules is shown in orange color. Bottom-panel: calculated evolution of Δ as a function of the film thickness (black line). (b) Magnified view of (a), including an additional RP-STO film on an STO substrate for which the stochiometry is not correct (purple). (c) Sketch of the RP structure with $n = 4$ u.c. of $SrTiO_3$ separated by single SrO atomic layers. (d) Corresponding experimental and simulated time evolution of Ψ.

substrate and therefore changes the ideal stoichiometry for the first layers. Another reason can be the formation of defects, which disturb the growth of RP-STO film with a well-defined structure. After overcoming the TZ, $d \sim 12$ nm, the simulation is almost in perfect agreement with the experiment data. This will be discussed below by presenting the strained RP films and the corresponding TEM images.

In figure 2(b), a magnified view for a part of the growth process, shown in figure 2(a), is presented. In addition, the data for a second film (purple color) is shown, which was grown with the same deposition parameters as for the first one (blue line), with the only exception of a 13% lower Sr-content in the solvent; this corresponds to the ideal stoichiometry value to grow $SrTiO_3$ films by conventional MAD. This deviation leads to clearly visible changes of the ellipsometry data, i.e. it results in a horizontal drift of Δ between the consecutive growth of a double Sr–O layer. Since the experimental errors (precursor weighting ~1.5%, syringes operation <0.2%) are relatively small and the optical alignment and the angle of incidence remained the same for those two samples, the differences in Δ can be completely attributed to a different film quality. The *ex situ* XRD confirms the absence of the desired RP phase for this 'poorly' grown film (not shown here). These non-stoichiometric ALE growth conditions within ALE were also reported for RP structures grown by MBE [19].

The corresponding evolution of the ellipsometric angle, Ψ, for the high quality RP-STO film on an STO substrate is displayed in figure 2(d). The atomic-layer oscillations are clearly resolved in the $\Psi(t)$ curve, although their amplitude is significantly smaller than in the $\Delta(t)$ curve as it is expected since measuring close to ϕ_B of material leads to a high sensitivity in $\Delta(t)$. Simulation and experiment follow the same trend, even though there is less agreement than for Δ (see figure 2(a)). A large deviation was observed for the time (film thickness) of $t > 500$ s ($d > 10$ nm), while for a thinner film the deviation is rather small.

The time evolution of Δ for the strained RP films grown on the LSAT and the $DyScO_3$ substrates are shown in figures 3(a) and (b). The difference between the refractive indices of these substrates and the RP film are larger than for the STO substrate, thus, leading to more pronounced interference effects (minima in $\Delta(t, d)$) already for thinner films, $d \sim 15$–20 nm. Nevertheless, for the strained films it is more difficult to obtain a good agreement between the model and the

Table 1. Model parameters used to describe the development of the ellipsometry signal. The refractive indices for bulk SrO and TiO_2 were taken at a wavelength of $\lambda = 589$ nm from the literature [18]. The values for atomic layer thicknesses were estimated to be $d_{SrO} = 0.21$ nm and $d_{TiO_2} = 0.19$ nm. The deviation of the adjusted values compared to the bulk values are shown in brackets. LSAT is the abbreviation of $(La_{0.3}Sr_{0.7})(Al_{0.65}Ta_{0.35})O_3$.

Substrate	$\tilde{n}_{SrO,bulk}/\tilde{n}_{TiO_2,bulk}$	$\tilde{n}_{SrO,adj.}/\tilde{n}_{TiO_2,adj.}$ 12.5 nm $< d <$ 50 nm	$\tilde{n}_{SrO,adj.}/\tilde{n}_{TiO_2,adj.}$ 7.1 nm $< d <$ 12.5 nm	$\tilde{n}_{SrO,adj.}/\tilde{n}_{TiO_2,adj.}$ $d <$ 7.1 nm
STO $\tilde{n} = 2.34,\ k = 0$ $\varphi = 61.22°$	1.871/2.612	1.869/2.645 (−0.1%/1.2%)	1.869/2.645 (−0.1%/1.2%)	1.869/2.645 (−0.1%/1.2%)
LSAT $\tilde{n} = 2.054,\ k = 0$ $\varphi = 62.0°$	1.871/2.612	1.83/2.61 (−2.2%/− 0.1%)	1.96/2.68 (4.8%/2.6%)	1.96/2.68 (4.8%/2.6%)
$DyScO_3$ $\tilde{n} = 2.1, k = 0$ $\varphi = 62.43°$	1.871/2.612	1.85/2.62 (−1.1%/0.3%)	1.91/2.67 (2.1%/2.2%)	2.02/2.74 (8.0%/5.0%)

experimental data. The first ~12 nm of the film seem to have a much higher refractive index than the rest of the RP film. This effect of a TZ we already observed in an RP film grown on a lattice matched STO substrate (see figure 2). In contrast, for strained RP films, the whole deposition was not possible to be simulated by using only one $\tilde{n}$-value for each Sr–O and Ti–O_2 atomic layer. Therefore, we described the TZ with one or two additional refractive indices for the case of a LSAT and $DyScO_3$ substrate, respectively (see table 1). For film thicknesses $d >$ TZ, the refractive indices used for the simulation match the bulk values taken from the literature better than for the case $d <$ TZ, suggesting a lower film quality in the first part ($d <$ TZ) of the film. Note that within the TZ, the refractive index changes probably not in a stepwise manner but rather gradually. Nevertheless, our model with the $\tilde{n}$-values shown in table 1 describes the experimental data quite well. The differences in the used $\tilde{n}$ for different substrates can be understood in terms of biaxial strain effect, i.e. tensile for $DyScO_3$ and compressive for LSAT. The strain is known to affect the band structure and, therefore, the refractive index of a given material, as was shown for strained STO thin films [20]. In the corresponding $\Psi(t)$ curves of the, RP films on LSAT (figure 3(c)) and $DyScO_3$ (figure 3(d)), atomic layer oscillations are observable, but are less pronounced than those in $\Delta(t)$ due to the same reason as for the RP film on an STO substrate, described above. However, the simulated $\Psi(t)$ curves oscillate weaker than the experimental data, and it was not possible to find any simulation parameters to satisfy simultaneously the $\Delta(t)$ and $\Psi(t)$ evolution. This indicates that even though several online information can be extracted from the measured ellipsometry data and the model accounts for most of the observed effects, nevertheless, this model seems to be not complete. The reason for that is, most probably, the fact that the Fresnel coefficients assume planar interfaces and, hence, the film roughness will not be represented by the equations used in this model. This could explain the progressively higher experimental values of Ψ as the deposition time continues and the film thickness increases, yielding probably a progressive increase of the film roughness.

Figure 3(e) shows the $\Delta(t)$ development at the early deposition stage of different RP films grown on $DyScO_3$ and LSAT substrates. One can see that the Δ-values of the first stack of 4 STO u.c. differ from those of the following repetitions (as was also seen in the case of an STO substrate). If we follow the Sr–O[Sr–O/Ti–O_2]$_{n=4}$ procedure, shown in the upper two panels of figure 3(e), it seems that the growth of the SrO atomic layers is suppressed until the extra SrO layer is deposited. For another sample, grown on LSAT, we immediately started the deposition with doubled SrO layers (magenta colored curve) and obtained a pronounced atomic layer oscillations from the very beginning of the growth. Apparently, the SrO extra layer plays an important role for the deposition of those oxides and catalyzes the growth on all used substrates. The corresponding simulation for an ideally grown RP-STO film on a LSAT substrate (see bottom curve of figure 3(e)) confirms this behavior.

Can this ellipsometry technique be equally suitable for the *in situ* monitoring during the growth of strongly absorbing materials? In figure 4, we simulated the evolution of the ellipsometric angles Δ and Ψ for a virtual RP thin film of Sr_2RuO_4 with $n = 1$ (SRO) epitaxially grown on an STO substrate. For a SRO film, the imaginary part of the refractive index, k, is significantly larger than zero at the wavelength of the laser beam, $\lambda = 632.8$ nm. For the calculation, we assumed that the SRO film is grown in the ALE-mode, i.e. by means of sequential deposition of the following atomic layers: [Sr–O/Sr–O/Ru–O_2]$_N$. The resulting atomic layer oscillations are clearly visible in the $\Delta(d)$ curve, whereas in the $\Psi(d)$ curve they are rather faint.

Next, we present and discuss the results of the *ex situ* structural characterization, carried out by XRD/XRR and TEM techniques, in order to find a correlation with the *in situ* measurements of optical ellipsometry. Figure 5(a) shows the XRD patterns for the samples grown on STO (blue curve), LSAT (green) and $DyScO_3$ (red), each with an underlying bare substrate (gray). All patterns show the desired out-of-plane epitaxy with *(00m)* x-ray peaks for the RP phase with $n = 4$ (labeled according to the diffraction order, m) and confirm

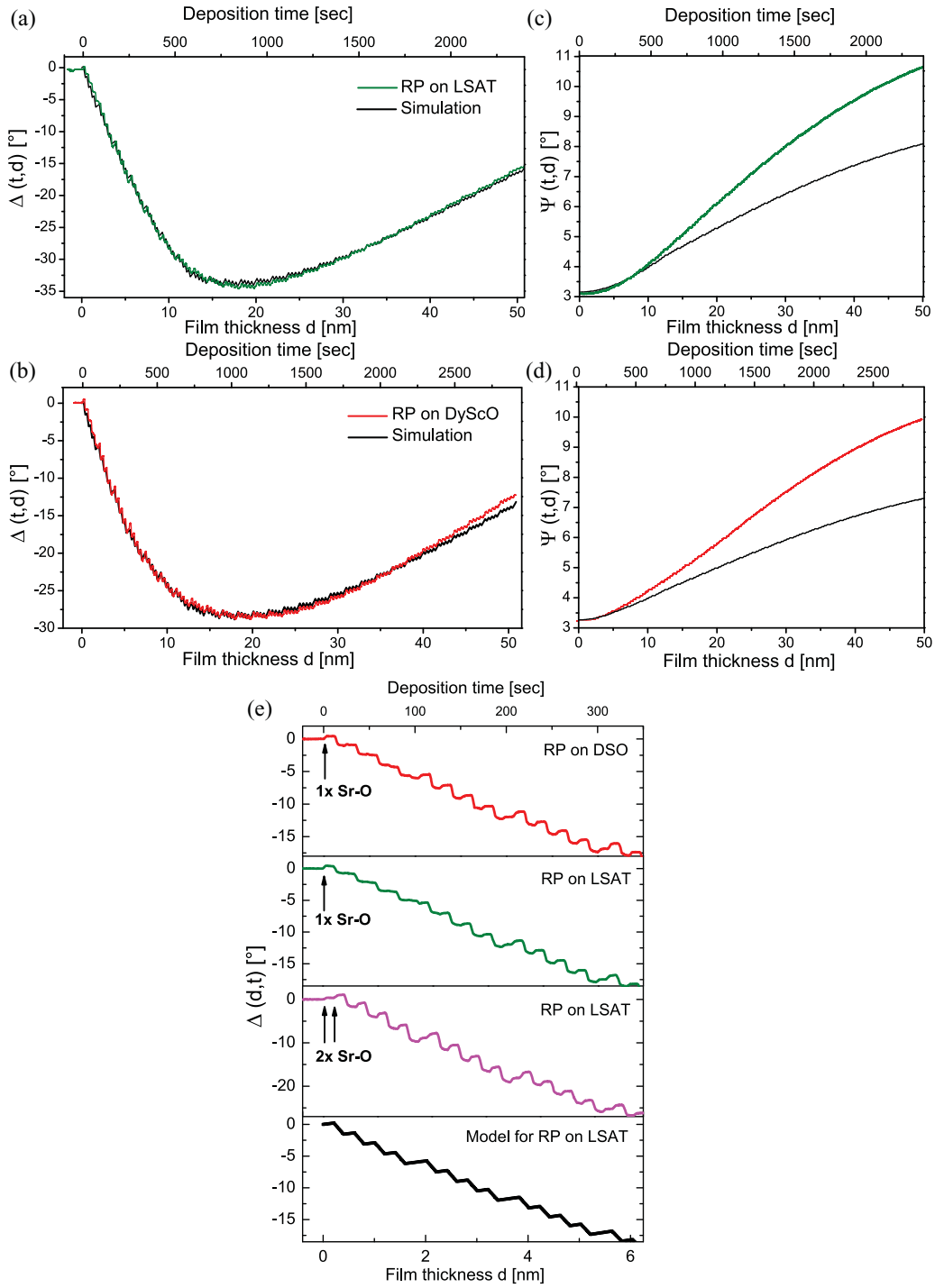

Figure 3. Ellipsometry signal of strained RP films on LSAT (in green color, (a) and (c)) and $DyScO_3$ (red, (b) and (d)) substrates together with the calculated curves (respectively for each substrate in black color). The crucial role of an additional SrO layer at the beginning of the growth is visible in (e).

the crystalline growth of these films. The out-of-plane lattice parameters (c-parameters) were calculated, using Bragg's law $2d_{(hkl)}\sin\theta = m\lambda$, from the slope of the linear fit to the different orders (see insets).

For the film on STO, the evaluated parameter, $c = 3.59(5)$ nm, agrees well with previous experimental and theoretical results [14, 22]. For the film on LSAT, the c-lattice constant is enlarged by about 0.6%. Such an increase is expected due to the compressive strain from the LSAT substrate with a 1% reduced in-plane lattice constant compared to STO. Similarly, for $DyScO_3$, which has a 1% larger in-plane lattice constant than STO and thus induces a tensile biaxial strain, we obtain a reduction of the c-axis lattice parameter by about −0.6%. The XRR curves for the RP films on LSAT and $DyScO_3$ are presented in figure 5(b) and show periodic oscillations, thus, confirming the large scale homogeneity and the smooth surfaces of the grown RP samples. From these oscillations, we derived the film thicknesses, $d = 51$ nm and 54 nm, respectively for the RP films grown on LSAT and $DyScO_3$. Note, that the contrast in the electron density between the RP-STO

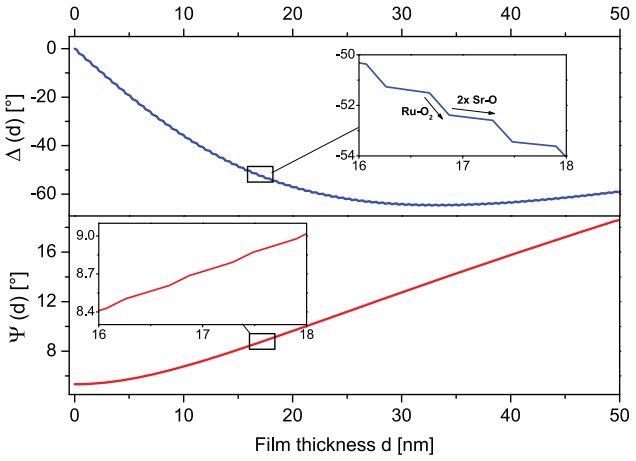

Figure 4. Theoretical optical response (Δ, Ψ) of Sr_2RuO_4 on STO(0 0 1) substrate by depositing single atomic layers of SrO and RuO_2 (see inset), with an angle of incidence of $\varphi = 70°$. The refractive index for RuO_2 was taken from bulk data [21] to be $\tilde{n} = 1.3 + 0.8j$.

film and the STO substrate is too low to observe these thickness oscillations.

In figures 5(c)–(e), the TEM images of an RP film grown on a LSAT substrate demonstrate a well-defined epitaxial growth with chemically sharp film/substrate and internal RP interfaces. Periodical ordering of the perovskite u.c. is visible along with continuous SrO-extra layers (figure 5(d)) that are marked with white arrows. The EELS image in figure 5(e) supports the achieved $n = 4$ stacking of the RP structure; here the Sr-atoms are colored in orange, the Ti-atoms in blue. The thickness of the film on the STO substrate could be estimated to be $d = 51(1)$ nm.

The vertical SrO defects as well as areas with pure STO or RP phases with different n, visible in the TEM images as well, were previously reported for MBE- and MAD-grown RP systems [14, 22, 23]. These can be explained by considering the Gibbs free energy of reaction $\Delta G = \Delta H - T\Delta S$, which will be lower for a mixture of RP phases than for a pure $SrO(SrTiO_3)_{n=4}$ phase film, due to the higher entropy S[22]. For instance, it has been shown that for $n > 3$ the RP films become thermodynamically unstable [24] and conventional solid state reaction methods fail to grow such heterostructures. Furthermore, vertically oriented SrO defects have low-energy interfaces [25].

Here, those defects mostly occur in the first ~12 nm of the grown film, which matches nicely the above mentioned TZ, observed by *in situ* ellipsometry (figures 2 and 3). This region appears to be independent of the substrate origin or the film thickness. Compared to the MBE-grown films, for which no such TZ was detected, the growth temperature within MAD is by about 200 °C higher, meaning that the growth kinetics might be of great importance.

We believe, that in the first few layers two-dimensional (2D) islands are formed due to a higher surface tension of the film compared to the substrate, as was previously reported [26]. As those 2D islands grow larger and finally start to overlap, they form mixed RP phases to decrease the Gibbs energy by the entropy term. After this TZ, a step-flow is stabilized, leading to an 'atomic layer-by-atomic layer' growth

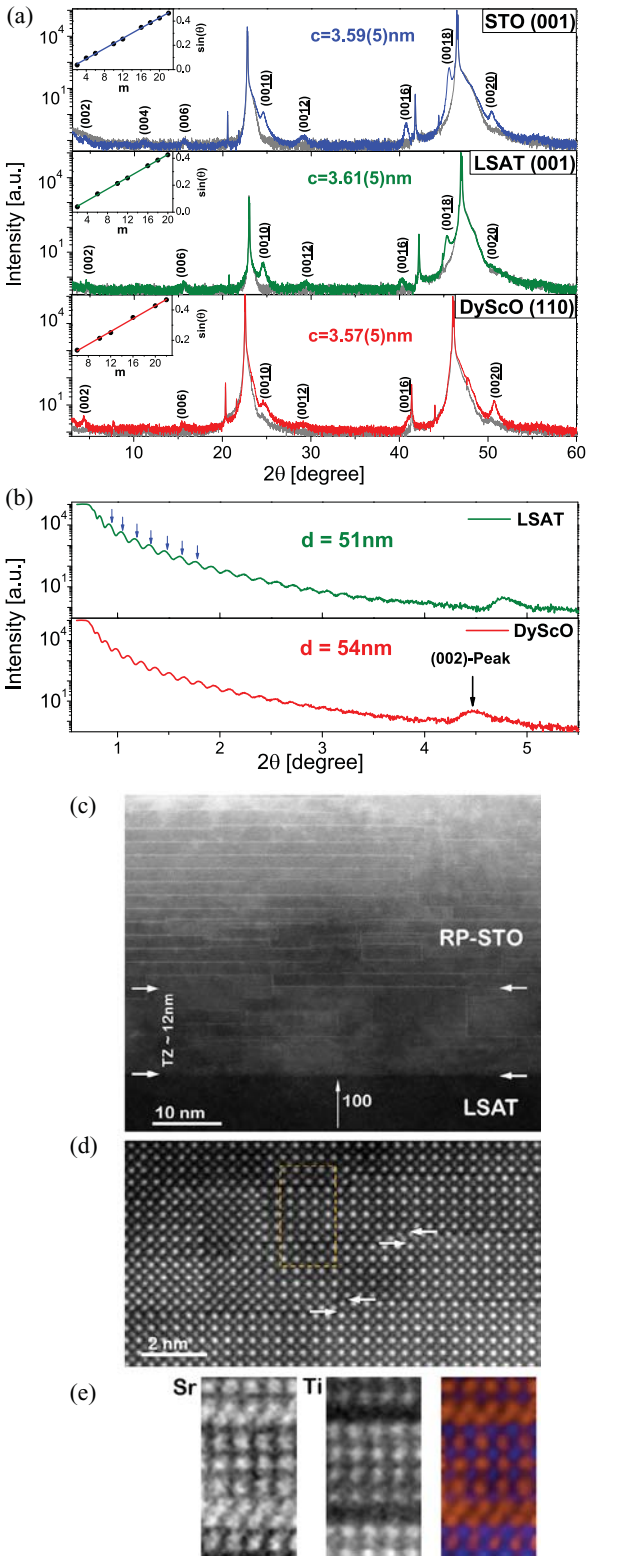

Figure 5. Structural analysis of RP-STO films. (a) XRD pattern of RP on STO(0 0 1) (blue), on LSAT (001) (green) and on $DyScO_3$ (110) (red). The respective spectra of each substrate are shown in gray color. The resulting RP-peaks are clearly visible. From Bragg's law (as shown in the insets) the c-lattice parameters (out-of-plane) were calculated. (b) XRR measurements: the thicknesses of the films grown on LSAT and $DyScO_3$ were calculated from the positions of the oscillation maxima (blue arrows). (c) Overview and (d) local HR-STEM image of RP grown on LSAT. Reproduced with permission [26]. (e) EELS mapping of strontium (orange) and titanium (blue) and their superposition. Continuous SrO-extra layers are clearly visible.

mode with natural stacking of Sr–O and Ti–O_2 atomic layers as it was designed for the RP-STO structure with $n = 4$.

4. Conclusions

We demonstrated the great potential of *in situ* ellipsometry for monitoring and studying thin film growth down to the scale of single atomic layers. Our ellipsometry setup allows monitoring the film growth down to the time scale of $\Delta t \sim 0.1$ s, which corresponds to a film thickness resolution of $\Delta d \sim 10^{-5}$ ML. Such an approach enables one to get an insight on the ALE of complex RP heterostructures with $n = 4$. The presence of a defect-rich transition zone, TZ ~ 12 nm, with vertically intergrown SrO layers and RP phases with $n \neq 4$ was directly evidenced by TEM in agreement with the ellipsometry data and ascribed to a relatively high deposition temperature within MAD. Furthermore, we found that the SrO extra layer acts like a 'growth catalyst' and induces the layered growth of these RP-STO films. The optical response during the ALE growth was modeled by using refractive indices for Sr–O and Ti–O_2 atomic layers, which were found to deviate from the corresponding bulk data by less than 1.2% for the unstrained film and by up to 8% for the strained films.

Acknowledgments

This work was financially supported by the EU FP 7 Project 'IFOX' and the Swiss National Science Foundation (SNF) via grant No. 200020-172611. We thank E Unger, S Hühn, A Cerreta, R de Andres Prada and E Perret for helpful discussions.

ORCID iDs

F Lyzwa https://orcid.org/0000-0003-1766-9547

References

[1] Ohtomo A and Hwang H Y 2004 *Nature* **427** 423
[2] Wang Q Y *et al* 2012 *Chin. Phys. Lett.* **29** 037402
[3] He S *et al* 2013 *Nat. Mater* **12** 605
[4] Bhattacharya A *et al* 2008 *Phys. Rev. Lett.* **100** 257203
[5] Haeni J H *et al* 2004 *Nature* **430** 758
[6] Renaud G *et al* 2003 *Science* **300** 5624
[7] Herman I P 2003 *Annu. Rev. Phys. Chem.* **54** 277–305
[8] Collins R W, Burnham J S, Sangbo K, Koh J, Lu Y and Wronski C R 1996 *J. Non-Cryst. Solids* **198–200** 981–6
[9] Zettler J-T, Wethkamp T, Zorn M, Pristovsek M, Meyne C, Ploska K and Richter W 1995 *Appl. Phys. Lett.* **67** 20
[10] Lee J-S and Masumoto Y 2000 *J. Cryst. Growth* **221** 111–6
[11] Zhu X D, Lu H B, Yang G-Z, Li Z-Y, Gu B-Y and Zhang D-Z 1998 *Phys. Rev.* B **57** 2514
[12] Chen F, Lu H, Thao T, Jin K-J, Chen Z and Yang G 2000 *Phys. Rev.* B **61** 10404
[13] Zhu X D, Fei Y Y, Wang X, Lu H B and Yang G Z 2007 *Phys. Rev.* B **75** 245434
[14] Jungbauer M, Hühn S, Egoavil R, Tan H, Verbeeck J, Van Tendeloo G and Moshnyaga V 2014 *Appl. Phys. Lett.* **105** 251603
[15] Moshnyaga V, Khoroshun I, Sidorenko A, Petrenko P, Weidinger A, Zeitler M, Rauschenbach B, Tidecks R and Samwer K 1999 *Appl. Phys. Lett.* **74** 2842
[16] Kawasaki M, Takahashi K, Maeda T, Tsuchiya R, Shinohara M, Ishiyama O, Yonezawa T, Yoshimoto M and Koinuma H 1994 *Science* **266** 1540–2
[17] Tompkins H G and Irene E A 2005 *Handbook of Ellipsometry* (Norwich, NY: William Andrew Publishing) (https://doi.org/10.1007/3-540-27488-X)
[18] Lide D R 2006–2007 *Handbook of Chemistry and Physics* 87th edn (Boca Raton, FL: CRC Press) (https://doi.org/10.1021/ja069813z)
[19] Nie Y F *et al* 2014 *Nat. Commun.* **5** 4530
[20] Tyunina M, Narkilahti J, Levoska J, Chvostova D, Dejneka A, Trepakov V and Zelezny V 2009 *J. Phys.: Condens. Matter* **21** 232203
[21] Goel A K, Skorinko G and Pollak F H 1981 *Phys. Rev.* B **24** 12
[22] Tian W, Pan X Q, Haeni J H and Schlom D G 2001 *J. Mater. Res.* **16** 7
[23] Lee C-H *et al* 2013 *Nature* **532** 502
[24] Tilley R J D 1977 *J. Solid State Chem.* **21** 293
[25] McCoy M A, Grimes R W and Lee W E 1997 *Phil. Mag.* A **75** 833
[26] Jungbauer M 2016 Gestaltung der elektronischen Korrelationen in Perowskit-Heterostrukturen auf atomarer Skala *Dissertation* Georg-August Universität Göttingen